



# Calculating the surface energies of crystals on a face-specific and whole particle basis: Case study of the $\alpha$ - and $\beta$ -polymorphic forms of L-glutamic acid<sup>☆</sup>

Thomas D. Turner<sup>a,1</sup>, Cai Y. Ma<sup>a,\*</sup>, Yuosef Al Ayoub<sup>b</sup>, Radoslav Y. Penchev<sup>b</sup>, Neil Dawson<sup>b</sup>, Martyn Ticehurst<sup>b</sup>, Robert Docherty<sup>c</sup>, Kevin J. Roberts<sup>a</sup>

<sup>a</sup> Centre for the Digital Design of Drug Products, School of Chemical and Process Engineering, University of Leeds, Leeds LS2 9JT, UK

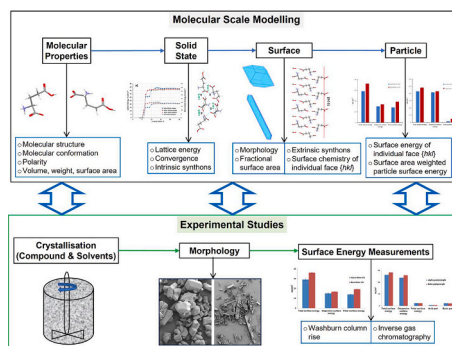
<sup>b</sup> Pfizer Worldwide Research and Development, Sandwich CT13 9NJ, UK

<sup>c</sup> School of Chemical and Process Engineering, University of Leeds, Leeds LS2 9JT, UK

## HIGHLIGHTS

- A methodology fusing experimental and computational workflows for the investigation of crystal surface energy has been presented.
- Molecular-scale (synthonic) modelling used to predict the surface energies of  $\alpha$  and  $\beta$  forms of L-glutamic acid on a face-specific and whole particle basis.
- Predicted surface energies are in good general agreement with measurements using IGC and Washburn capillary rise techniques.
- Calculated surface energies have the same trend as those from experiments though they are higher than the experimental values, which are consistent with literature findings.
- The overall molecular modelling approach demonstrates its application in designing crystal habit for optimising particle surface energies for product formulatability particularly in early phase process development.

## GRAPHICAL ABSTRACT



**Abbreviations:**  $A, B$ , Atom-atom parameters;  $A_i^{hkl}$ , Fractional surface area of a habit face ( $hkl$ ) for  $i^{\text{th}}$  form;  $d_{hkl}$ , Thickness of the growth step layer;  $E_{latt}$ , Lattice energy / kcal mol<sup>-1</sup>;  $E_{sb}$ , Slice energy / kcal mol<sup>-1</sup>;  $E_{att}$ , Attachment energy / kcal mol<sup>-1</sup>;  $hkl$ , Miller index;  $i, j$ , Atom in the central molecule,  $k^{\text{th}}$  surrounding molecule;  $M_i^{hkl}$ , Multiplicity of a specific habit face for  $i^{\text{th}}$  form;  $N$ , Number of surrounding molecules;  $n$ , Total number of atoms in the central molecule;  $n'$ , Total number of atoms in each of the surrounding molecule;  $N_A$ , Avogadro's constant;  $q_i, q_j$ , Partial, atomic point charges on atom  $i, j$ ;  $r_{ij}$ , Inter-atomic distance between atoms  $i$  and  $j$ ;  $V_{cell}$ , Unit cell volume;  $Z$ , Number of formula units within the crystallographic unit cell;  $\gamma^{hkl}$ , Surface energy of individual crystal surface ( $hkl$ );  $\gamma_{particle}$ , Surface area weighted overall particle surface energy;  $\epsilon_{hkl}$ , Anisotropy factor; API, Active pharmaceutical ingredients; FE-SEM, Field emission scanning electron microscope; IGC, Inverse gas chromatography; LGA, L-glutamic acid; SEM, Scanning Electron Microscopy; WCR, Washburn capillary rise.

<sup>☆</sup> Dedicated to the life and works of Reg Davies.

\* Corresponding author.

E-mail address: [C.Y.Ma@leeds.ac.uk](mailto:C.Y.Ma@leeds.ac.uk) (C.Y. Ma).

<sup>1</sup> School of Chemistry, University of Leeds, Leeds LS2 9JT, UK.

<https://doi.org/10.1016/j.powtec.2024.120276>

Received 19 July 2024; Received in revised form 6 September 2024; Accepted 10 September 2024

Available online 11 September 2024

0032-5910/© 2024 The Authors. Published by Elsevier B.V. This is an open access article under the CC BY license (<http://creativecommons.org/licenses/by/4.0/>).

## ARTICLE INFO

## Keywords:

Molecular modelling  
Synthonic engineering  
Surface energy  
Surface chemistry  
Lattice energy  
L-glutamic acid  
Attachment energy

## ABSTRACT

Molecular-scale modelling for predicting surface energies on a face-specific and whole particle basis is applied to all the crystallographically-independent surfaces of L-glutamic acid forms. The predicted data is found to be in good general agreement with measured surface energies using inverse gas chromatography and Washburn capillary rise techniques with the former revealing higher values compared to the prediction, perhaps consistent with the polar (zwitterionic) nature of this material. This fusion of experimental and computational data provides a high-fidelity definition of the face-by-face breakdown of the energetic anisotropy of the crystals. There is increasing industrial interest in defining the potential impact of whole particle properties on the performance of formulated drug product and their manufacturability especially as the community accelerates the molecule to medicine journey. The overall molecular modelling approach highlights its application in designing ingredients for optimising face-specific particle surface energies for product formulatability particularly in early phase process development.

## 1. Introduction

In contrast to simple elemental and inorganic materials, organic crystalline molecules such as pharmaceuticals can often have quite anisotropic molecular properties and, when crystallised, the resultant material can also display significant anisotropy, most notably in their surface properties. Diagrammatically, superimposing an outline of the crystal's external morphology onto its bulk crystallographic structure can reveal the differences in the surface chemistry of the crystal habit surfaces reflecting the formation of the bulk intermolecular interactions exposing different functional groups at the crystal surfaces. Such surface properties are important not only individually as active pharmaceutical ingredients (API), but also when formulated with other materials or excipients into solid dosage forms and suspension products [1–3]. In this, the individual crystal habit surfaces may interact differently when exposed to the presence of air, moisture, solvents, impurities, excipients and processing equipment. If uncontrolled, this behaviour can lead to batch-to-batch variability, which can impact in turn upon the behaviour of crystals during the API and drug product (DP) manufacturing processes, through unit operations such as crystallisation, isolation, drying, blending and compaction. These changes can also impact upon the performance of the formulated material in the marketed product, notably in terms of drug product stability to physical and chemical transformation and as well as its in-vivo dissolution properties and hence its bioavailability [1–3].

There are two key drivers in the pharmaceutical industry that dictate interest in this area namely the need to accelerate the molecule to medicine journey and to reflect the impact of digital transformation. The acceleration of product development means that the timelines associated with drug development have been significantly reduced resulting in a greater focus at the API:DP interface where a classical iterative approach can be problematic in terms of time and batches required to evolve the necessary knowledge and understanding. Digital transformation across industry means that the community is attempting to use digital design tools to transform the molecule to medicine journey with fused computational and experimental workflows which are nowadays seen as a crucial step towards simulation-led design [4–6].

The properties of pharmaceutical powders reflect the bulk and surface crystallography of the material and, in turn, the nature of intermolecular interactions both within the bulk material (intrinsic synthons) and the same when terminated at the crystal surfaces (extrinsic synthons). The strength and directivity of these synthons is very much a reflection of the dominating types of unsaturated functional groups within the extrinsic synthons which are hence available for interaction at the crystal habit surfaces leading to different type of intermolecular interactions, i.e. H-bond, electrostatic or van der Waals. It is these that direct the crystal face's properties such as their relative growth rate during crystallisation, surface wettability and whether the particle would exhibit e.g. a hydrophilic or hydrophobic nature in the presence of other ingredients within the formulated product. Such differences in

surface properties are also manifested in the differences in the surface energies of the different crystal habit faces and through this the net surface energetics of the whole crystal particle. The latter can be estimated as a surface area weighted sum of the surface energies of the individual surfaces.

Importantly, inherent within the above concept, is that when the morphology of the particle changes, e.g. due to processing variations, the overall particle surface energy can also change. The position of certain functional groups relative to surface topology of the surfaces is equally important, as a stepped or even rough surface at the molecular scale will typically have more binding sites and hence a lower barrier for surface adsorption in comparison to the more closely-packed smooth planes. Hence, a detailed knowledge encompassing a combination of surface energetics, topological structure and the chemistry of the exposed functional groups on the habit surfaces is a vital resource for both process and product design. Through this, an assessment of the likely behaviour of crystal particles within the external environment can be understood and predicted in terms of how the API or excipient particles might cohesively or adhesively interact with themselves and other materials respectively both during processing and within the formulated drug product [7–9].

L-glutamic acid (LGA) is an organic material with pharmaceutical applications whose chemical and physical properties are well understood. LGA has two polymorphs comprising the prismatic-shaped metastable  $\alpha$ -form and needle-like stable  $\beta$ -form [10] and has been widely used as a model compound in crystallisation process research [10–29]. In-situ single crystal growth of LGA in growth cell systems has been performed to measure facet growth rates (e.g. [28,30–32]). The use of these online imaging systems have provided powerful approaches to study crystallisation processes including crystal growth kinetics within a population of crystals (e.g. [11,15–21,33]) and also the effect of operating conditions on the processing behaviour including the variations of crystal size and shape during the unit operations (e.g., [12,14,22,24,29,34–36]).

Molecular-based simulation approaches have been used to understand and predict crystal morphology associated with crystal surface chemistry and facet growth [1] with, for example, molecular modelling software such as HABIT98 [37,38] being used for predicting the crystal lattice energy, inter-molecular interactions (synthons), relative growth rates and crystal morphology, for surface binding propensity, etc. Molecular dynamics simulations have been utilised to investigate the energetic balance between solute and solvent intermolecular interactions (e.g., [39–41]) and solution-mediated intramolecular hydrogen bonding [42] and the assembly of synthons within the solution state [43], and also for studying crystal nucleation and growth in the solution state [44,45]. A surface cleaving technique [46] has been implemented within a molecular dynamics simulation framework and used to calculate the surface energies of  $\beta$ -form D-mannitol crystal with the results being compared with experimental data from inverse gas chromatography (IGC) measurements [47]. Despite this, there have been relatively

few studies of the effect of variations in the particle production processes upon surface crystallinity, particle adhesion and cohesion for inhalation products. The integrated study of the interactions between alpha lactose monohydrate ( $\alpha$ LMH) and terbutaline sulphate (TBS) [9,48,49] has demonstrated the potential of such studies. The work carried out has provided some fundamental insight as regards the surface properties of  $\alpha$ LMH, TBS and their interactions from a molecular-scale standpoint, particularly in terms of characterising the external morphology, surface chemistry and particle surface energy, and their link to the adhesive and cohesive interactions between API and excipient for achieving effective aerosolization, efficacy, lung delivery of inhalation drugs [9,48,49].

In a previous paper [50], the solvent-mediated crystal morphologies of both  $\alpha$  and  $\beta$  forms of L-glutamic acid were examined through the application of a digital mechanistically based workflow encompassing calculations of crystal lattice energy and its constituent intermolecular synthons, their interaction energies, and their key role in understanding and predicting crystal morphology as well as assessing the surface chemistry, topology, and solvent binding on crystal growth surfaces. Both  $\alpha$  and  $\beta$  forms were found to display an extensive network of coulombic and hydrogen-bonding interactions, hence classified as three-dimensionally hydrogen-bonded materials [50]. Specifically, it was found that the  $\alpha$ -form has a more isotropic distribution of the dominant synthons amongst its attachment energies, whilst the  $\beta$ -form shows a much more anisotropic distribution of the dominant extrinsic synthons between the habit faces. This directly affects the relative crystal growth rates of the  $\alpha$ - and  $\beta$ -LGA faces, rationalising the observed prismatic and needle-like morphologies. The faster convergence of lattice energy for the  $\alpha$  form was found to be consistent with its formation of smaller stable molecular clusters when compared to the  $\beta$  form, in agreement with the calculated cluster energy as a function of size [23]. The analysis of intrinsic synthons within the solid-state identified the strongest intermolecular interactions for both  $\alpha$  and  $\beta$  forms in particular highlighting the importance of the charged zwitterionic functional groups in terms of their total contributions to the intermolecular energy [50]. Detailed knowledge, provided by a fundamental intermolecular (synthonic) assessment, has thus been shown to deliver useful baseline data for improved understanding of particle surface properties and associated interparticle interactions. A summary of the challenges in this area was highlighted by a map connecting API attributes back from the drug product showed the opportunity of fusing face specific simulation with bulk property experimental measurements [2].

Experimental determination of surface properties of powdered crystalline materials can include, for example, inverse gas chromatography (IGC) [51,52], contact angle measurements and wettability [53] using Washburn capillary rise [54]. Overall, it has been found that accurate experimental determination of surface energy of crystalline powders can be challenging, e.g. the capillary rise method may not always provide reliable results of contact angles [55,56]. Surface energy measurements from IGC using both polar and apolar probes [57–61] have, however, been found to be particularly useful in studies of the crystallinity, surface energy and surface properties of particles. However, powder characterisation using IGC has revealed a number of problematic issues such as sample preparation-dependency, large sample sizes (e.g. for micronised materials ~50–100 mg and for coarse particles more than 2 g of sample are required typically) [62], time utilisation and hence high cost. Variability in IGC measurements has also been reported [63–65] and the technique, even with finite dilution analysis is limited to surface coverage of up to 10–15 % of the total sample surface area. Hence, if results are to be useful, there is a clear need for a better molecular-scale understanding of both the sources of variability and the impact of surface features on IGC measurements. Generally, current techniques do not provide the capability to routinely measure surface energies on a crystal habit face-specific basis and therefore cannot easily assess face-specific surface energy variations due to crystal morphological changes.

In this paper, an integrated study encompassing both computational prediction and experimental determination of the surface energies of

LGA as a function of its solid form properties (morphology and polymorphic form) is presented. LGA is being used as a model material to demonstrate the type of analysis that could be valuable to apply to API and/or excipient during drug product development. The surface energy determined directly links with drug particulate-interactions and the associated intrinsic powder properties for achieving optimum cohesive and adhesive interactions between API and excipient, hence not only for effective aerosolization, lung delivery of inhalation drugs [9,48,49] but also for more general applications in the formulation process design of other APIs such as tableting and tablet dissolution. Here, an overall workflow is provided that embraces the fusion of both computational and experimental workflows to provide a key driver within the pharmaceutical industry over the next few years.

## 2. Materials and methods

A diagrammatic route map summarised in Fig. 1 provides a specific example of the surface properties workflow providing an overview of the main features of the modelling and experimental methods used. The workflow encompasses the components for the surface energy predictions of crystalline materials (including the predictions of molecular properties, crystal lattice energy and intrinsic synthons, crystal morphology and surface chemistry with extrinsic synthons, surface energies of crystal faces and also the latter for a whole particle), for crystallised crystals together with surface energy measurements using two methods (Washburn capillary rise (WCR) and inverse gas chromatography (IGC)), with the interactions and comparisons between the predictions and measurements highlighted.

### 2.1. Experimental studies

#### 2.1.1. Materials

L-glutamic acid (99 %) was used as supplied by Sigma Aldrich. Deionised water was used for recrystallization of L-glutamic acid. Decane, nonane, octane and heptane were purchased from Sigma-Aldrich, UK. Ethyl acetate and dichloromethane were obtained from Fischer Scientific, UK. Diiodomethane was purchased from Alfa Aesa, UK. All materials were used as supplied without any purification.

#### 2.1.2. Preparation of L-glutamic acid $\alpha$ and $\beta$ forms

L-glutamic acid was recrystallized to prepare the two polymorphic forms;  $\alpha$  and  $\beta$ . This was carried out using a HEL Autolab 0.5 L jacketed vessel with temperature control provided through a Julabo F32 with attached PT100 thermocouple which was inserted into the reactor. The contents of the vessel were agitated at constant stirring of 200 rpm with a three blade pitched impeller. To recrystallize the meta-stable  $\alpha$ -form, a solution of l-glutamic acid in deionised water at 30 g kg<sup>-1</sup> concentration was prepared in the reactor. This was then subjected to a heating cycle from 25 °C to a holding temperature of 90 °C for one hour to allow full dissolution of solids. The solution was then cooled at 0.7 °C min<sup>-1</sup> to a lower holding temperature of 5 °C, where the recrystallized solids were isolated using vacuum filtration and dried in an oven at 40 °C. To obtain the  $\beta$ -form solids this methodology was repeated however the solution concentration was increased to 50 g kg<sup>-1</sup> and the cooling rate decreased to 0.1 °C min<sup>-1</sup>.

#### 2.1.3. Solid form characterisation

Powder X-ray diffraction (PXRD) was used for polymorph characterisation on a regular basis for confirming the polymorphic purity of the two phases of LGA. This was carried out using a Bruker D8 advanced X-ray diffractometer which used Cu K $\alpha$  radiation and a germanium primary monochromator in Bragg-Brentano reflection geometry. The step size used was 0.033 2 $\theta$  and the step time used was 0.7 s per step over a 2 $\theta$  range of 4–39.8 2 $\theta$ . The detector used was a Vantec-1 position sensitive detector.

Scanning Electron Microscopy (SEM) was used for morphological

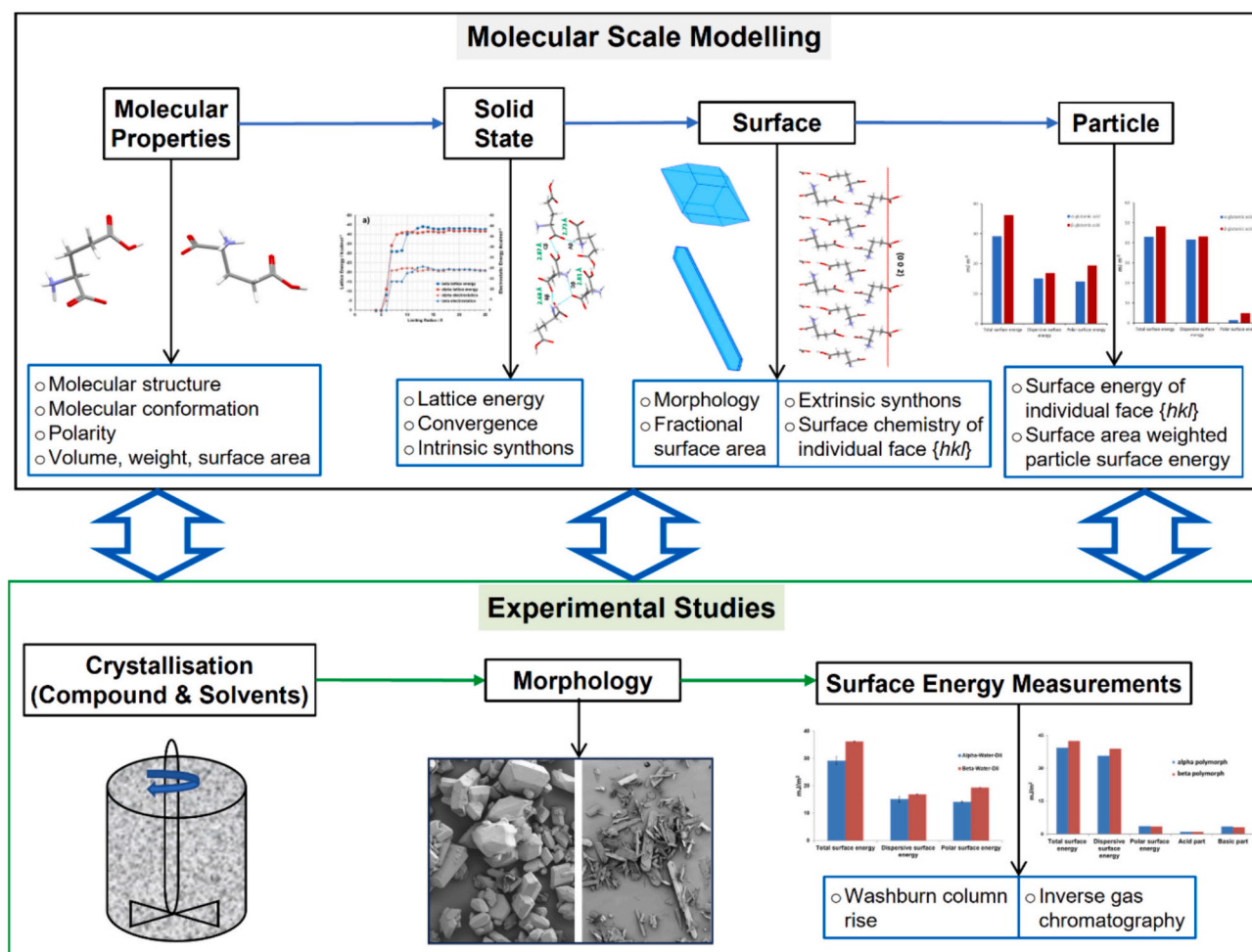


Fig. 1. A route map from molecular and crystallographic structure to surface energy calculation with combined experimental workflow.

characterisation. Samples were prepared by adhering about 1 mg of the powder from each specimen onto adhesive Sticky Tabs placed on separate 12.5 mm diameter aluminium pin stubs. Excess powder was removed by tapping the stubs sharply and then gently blowing loose particles off with a jet of particle-free compressed gas. The prepared specimen stubs were sputter coated with a thin (approximately 10 nm) deposit of platinum using a Quorum Q150TS coating unit operated at 20 mA for 1 min using argon gas. The specimens were examined using a Carl Zeiss SMT SUPRA 40VP field emission scanning electron microscope (FE-SEM). The FE-SEM was operated at high vacuum with an accelerating voltage of 3 kV, a specimen working distance of 12 mm. Secondary electron images were recorded at magnifications of 50 $\times$  and 200 $\times$ .

#### 2.1.4. Surface energy measurements

To validate the prediction of the particle surface energy model for the two polymorphs of LGA, the bulk powder surface energy was determined using two industry standard experimental approaches; inverse gas chromatography and the Washburn capillary rise method.

Surface energy was measured using inverse gas chromatography - Surface Energy Analyser II (IGC - SEA, Surface Measurement Systems, London, U.K). The samples were packed into 4 mm pre-silanised glass columns. The columns were pre-conditioned at 30 °C and 0 % RH using helium carrier gas) at a flow rate of 10 standard cubic centimetres per minute for 120 min and these conditions were maintained throughout the experiment duration. A range of non-polar probes (decane, nonane, octane and heptane) and polar probes (ethyl acetate and dichloromethane) were injected at range of surface coverages ranging from

0.025 to 0.15 ( $\text{nm}^{-2}$ ). The column dead volume was determined using methane. Surface Energy Analysis Software (v1.4.3.0, SMS Ltd., UK) was utilised for the data analysis. In this, the Schultz approach and Della Volpe scale with Peak Max Time parameter were used to calculate the surface energy of the samples [66]. The acidic (Lewis acceptor) and basic (Lewis donor) parts of polar surface energy were determined from the injection of two monopolar probes with opposite polarities: dichloromethane and ethyl acetate, respectively, as detailed in literature [67].

The contact angle of each test sample was determined based on the capillary rise method using a Krüss K100 Tensiometer (KRÜSS GmbH, Germany). The samples were packed into a tube vessel (provided by Krüss) and then a 50 g weight tool was applied to the sample for 60 s. The capillary constant of the material was determined in triplicate in heptane. The contact angle of water and diiodomethane were then measured in triplicate. The free surface energy of the samples was calculated using the Owens-Wendt-Rabet-Kaelble approach provided by the Krüss Laboratory Desk Interface software (Version 3.2.2.2926). Note that the liquid (solvent) was put onto a powder sample to measure the zero angle to the angle created by the meniscus of the liquid. In this study, the contact angles in heptane, water and diiodomethane were measured to obtain the nonpolar and polar components for determining particle surface energy as described above.

#### 2.2. Molecular and crystallographic modelling

The crystal structures of the  $\alpha$ -form (CSD refcode LGLUAC02) [68] and  $\beta$ -form (CSD refcode LGLUAC01) [69] for L-glutamic acid were

obtained from the Cambridge Structural Database (CSD). These were optimised using the Forcite module of Materials Studio [70], where the unit cell parameters and molecular positions were allowed to relax and the intermolecular features such as bond, length, angles and conformations were held rigid. The forcefield used was Dreiding [71] with the partial electronic charges on the atoms being calculated using the Gas-teiger method [72,73].

### 2.2.1. Calculating the strength of intermolecular interaction and the crystal lattice energy

The intermolecular interactions which contribute to the stabilisation of two lattice structures for the two polymorphs after optimisation using Forcite module [70] were analysed using HABIT98 [37,38] utilising an atom-atom approach [74] for which a range of atom-specific force-field parameters are readily available e.g. the Lennard Jones 6–12 potential which can be coupled with a coulombic function to deal with the effect of molecular polarisation. The lattice energy,  $E_{latt}$ , was calculated from the strength of these intermolecular interactions (synthons) using a Momany potential set [75] together with the partial atomic charges calculated in MOPAC [76] [77]. The lattice energy ( $E_{latt}$ ) was computed by constructing a network of unit cells and calculating the intermolecular interactions at increasing sphere sizes expanding from a central molecule, providing a measure of the structure's cohesively and strength, thus:

$$E_{latt} = \frac{1}{2} \sum_{k=1}^N \sum_{i=1}^n \sum_{j=1}^{n'} -\frac{A_{ij}}{r_{ij}^6} + \frac{B_{ij}}{r_{ij}^{12}} + \frac{q_i q_j}{r_{ij}} \quad (1)$$

where  $A$  and  $B$  are atom–atom parameters,  $i$  is an atom in the central molecule,  $j$  is an atom in the  $k^{th}$  surrounding molecule,  $N$  is number of surrounding molecules,  $n$  is total number of atoms in the central molecule,  $n'$ , is total number of atoms in each of the surrounding molecule,  $q_i$  and  $q_j$  are partial, atomic point charges on atoms  $i$  and  $j$ , and  $r_{ij}$  is interatomic distance between atoms  $i$  and  $j$ . Summing up all such interactions will converge as the interaction energy increases to yield the crystal lattice energy. As the strength of the interactions is strongly inversely dependent of the intermolecular distance, the lattice energy summation process converges typically at distances between 30 and 40 Å. The calculated lattice energy was subdivided into the interaction's constituent van der Waals (vdW), hydrogen bonded and polar (electrostatic) energies, hence the corresponding dispersive (vdW) and polar surface energies in the latter calculations.

The convergence of the lattice energy was assessed by 1 Å step wise calculations between 5 and 25 Å of the calculation sphere. This well-established approach has also been successfully applied to other studies of LGA (e.g. [1,50,78]) and other compounds including entacapone [79], para-aminobenzoic acid [39,41,80], terbutaline sulfate [48], quercetin [52], tolafenamic acid [81], ritonavir [42,82].

In the literature [50,78], cross-correlating the calculated lattice energy to the known experimental sublimation enthalpy of the  $\beta$ -form LGA [83] and the proton transfer energy (reflecting the zwitterionic nature of LGA in its solid-state form) [84] was utilised to assess the suitability of the potential used, demonstrating a pleasing agreement in terms of relative polymorphic stability, lattice energy validation and structural change following minimisation. Hence this was found to be sufficient for the purposes in this and previous [50,78] studies.

### 2.2.2. Partitioning the intermolecular interactions

The pairwise intermolecular interactions were partitioned between the slice,  $E_{st}$ , and attachment,  $E_{att}$ , energy contributions, as described in Eq. (2) [85]. The former reflects those contributing the bulk structural stability (intrinsic synthons) whilst the latter reflects those terminated at the external crystal habit surfaces (extrinsic synthons) and hence energetically surface active, thus:

$$R_{hkl} \propto E_{att}^{hkl} = E_{latt}^{hkl} - E_{st}^{hkl} \quad (2)$$

where  $E_{st}^{hkl}$  is the sum of the intermolecular interactions that lie parallel and within the lattice plane spacing,  $d_{hkl}$ , and  $E_{att}^{hkl}$  is the energy released upon addition of a growth slice of  $d_{hkl}$  to a growing crystal surface [86,87]. The calculated values of  $E_{att}^{hkl}$  were taken as a proportional measure of the relative growth rates of the crystal surfaces [86,88] (as shown in Eq. (2)) and used to predict a particle morphology through a Wulff plot [89,90] using CCDC's Mercury software. The predicted crystal habit [50] based on the attachment energy model also enabled calculation of the fractional surface areas of individual crystal habit faces  $\{hkl\}$ . The latter was calculated using Materials Studio software [70].

### 2.2.3. Calculation of surface energy

The surface energy ( $\gamma^{hkl}$ ) of a given crystal surface ( $hkl$ ), can be directly calculated from the attachment energy of this surface [86,87], thus:

$$\gamma^{hkl} = \frac{Z d_{hkl} |E_{att}^{hkl}|}{2 N_A V_{cell}} \quad (3)$$

where  $Z$  is the number of molecules per unit cell,  $d_{hkl}$  is the thickness of the growth step layer,  $N_A$  is Avogadro's constant, and  $V_{cell}$  is the unit cell volume. The dispersive and polar components of the surface energy were calculated from the surface energy contribution from the van der Waals and coulombic components, respectively. The  $\gamma^{hkl}$  is also referring to the total surface energy of one reticular area of the specific crystallographic plane as  $\gamma_{Total}$  where  $\gamma_{dispersive}$  and  $\gamma_{coulombic}$  are the dispersive (vdW) and coulombic (polar) components respectively.

The 'surface area weighted'  $\gamma_{Total}$ ,  $\gamma_{dispersive}$  and  $\gamma_{coulombic}$  were calculated by considering the fractional surface area of each face and its multiplicity on the morphology models, hence the overall net surface energy of a whole crystal particle,  $\gamma_{particle}$ , for a given morphology with multiple  $hkl$  planes and its relative dispersive and coulombic components being simply a summation of these values according to Eq. (4) through Eq. (3):

$$\gamma_{particle} = \sum_{i=1}^n \gamma_i^{hkl} A_i^{hkl} M_i^{hkl} = \sum_{i=1}^n \left( \frac{Z E_{att}^{hkl} d_{hkl}}{2 N_A V_{cell}} \right) A_i^{hkl} M_i^{hkl} \quad (4)$$

where  $n$  is the number of forms ( $\{hkl\}$ , i.e. family of faces),  $\gamma_i^{hkl}$  is surface energy of individual crystal surfaces,  $M_i^{hkl}$  is the multiplicity of the specific habit face (i.e. the number of symmetry equivalent faces) and  $A_i^{hkl}$  is the fractional surface area of the habit face [1,48,79,91].

## 3. Results and discussion

### 3.1. Calculated particle surface energies

The  $\alpha$ -form of L-glutamic acid was crystallised as well-defined prismatic-like crystals as shown in the SEM image in Fig. 2a), whereas the  $\beta$ -form was found to crystallise with a needle-like morphology, Fig. 2b). Morphological models of the crystal habit for these two polymorphs were created using a modified attachment energy approach and highlighted in Fig. 2c) and d) for  $\alpha$ - and  $\beta$ -forms respectively. The  $\alpha$ -form morphology was found to be dominated by large  $\{111\}$  and  $\{002\}$  surfaces whereas the  $\beta$ -form crystals were found to be formed through elongation of the  $a$ -axis through fast growing  $\{111\}$  surfaces together with a side  $\{011\}$  surface and slow growing  $\{002\}$  surfaces which dominate the morphology.

The calculated surface energies using the attachment energy approach are provided in Table 1 for the  $\alpha$ - and  $\beta$ -forms with their dispersive ( $\gamma_{dispersive}$ ) and polar ( $\gamma_{coulombic}$ ) components and also surface area weighted ones.

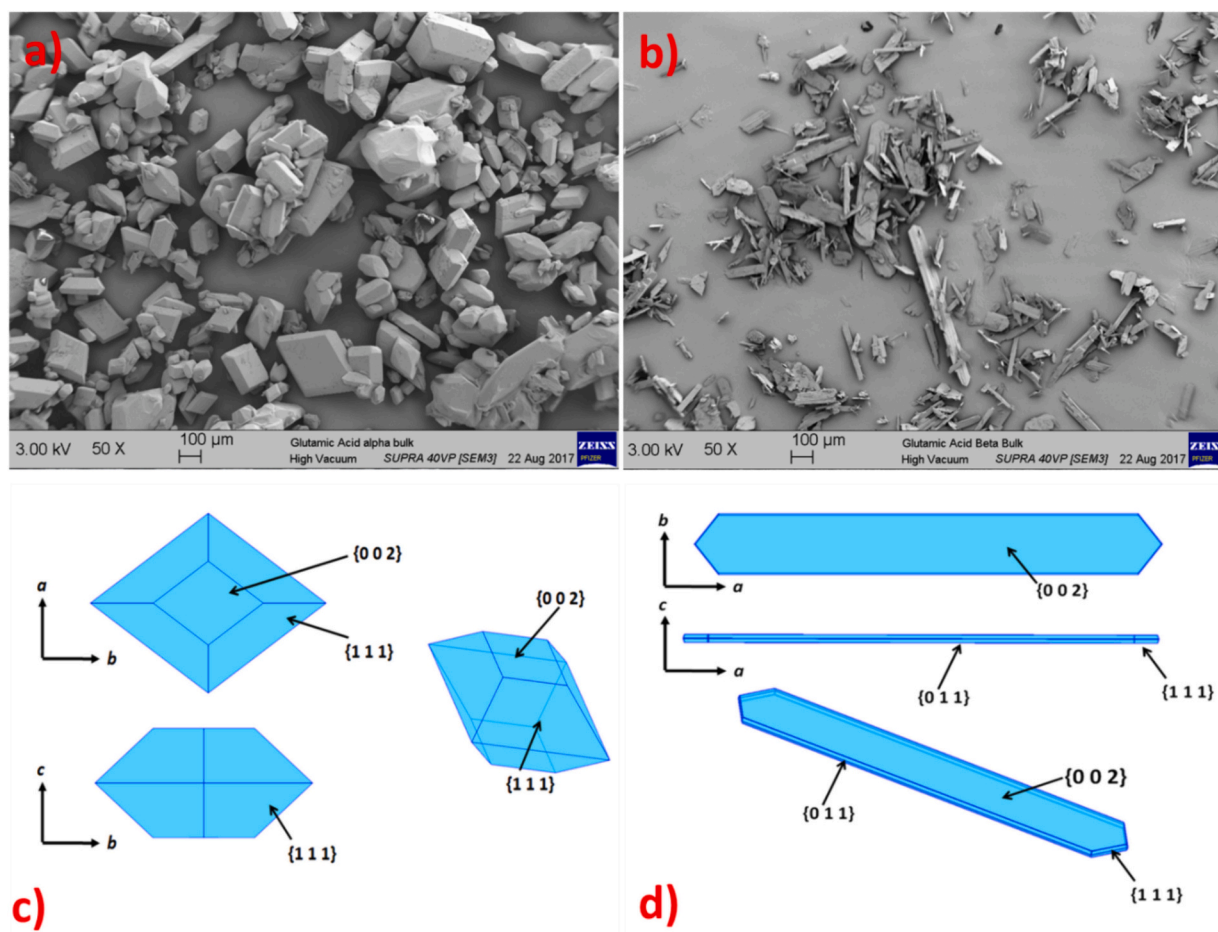


Fig. 2. a) SEM images of the prismatic  $\alpha$ -form crystals as obtained from fast cooling crystallisation experiments b) SEM images of the needle-like  $\beta$ -form crystals as obtained from slow cooling experiments c) morphological model of the  $\alpha$ -form highlighting the important  $\{111\}$  and the  $\{002\}$  surfaces, d) morphological model of the  $\beta$ -form dominated by the slow growing  $\{002\}$  surface.

Table 1

Surface energy calculation for the  $\alpha$ - and  $\beta$ -forms of L-glutamic acid, highlighting the dispersive and coulombic components of the surface energy and the overall particle surface energy with dispersive and coulombic components.

Face	$d_{hkl}$ / Å	Face Multiplicity	Attachment Energy / kcal mol <sup>-1</sup>	$\gamma_{Dispersive}$ / mJ m <sup>-2</sup>	$\gamma_{Coulombic}$ / mJ m <sup>-2</sup>	$\gamma_{Total}$ / mJ m <sup>-2</sup>	% Surface Area	Surface Area Weighted Surface Energy (Dispersive) / mJ m <sup>-2</sup>	Surface Area Weighted Surface Energy (Coulombic) / mJ m <sup>-2</sup>	Surface Area Weighted Total Surface Energy / mJ m <sup>-2</sup>
<b><math>\alpha</math> polymorph</b>										
$\{111\}$	4.92	8	-21.28	125.06	94.06	219.12	86.64	108.38	81.51	189.90
$\{002\}$	4.45	2	-25.79	138.96	101.14	240.10	13.34	18.53	13.49	32.01
<b>Whole crystal</b>								<b>126.91</b>	<b>95.00</b>	<b>221.91</b>
<b><math>\beta</math> polymorph</b>										
$\{111\}$	3.92	8	-24.40	138.96	79.73	218.69	2.16	3.02	1.73	4.76
$\{002\}$	8.92	2	-24.03	236.23	253.87	490.10	85.82	202.71	217.85	420.55
$\{011\}$	6.40	4	-18.61	145.91	126.40	272.31	12.02	17.53	15.18	32.71
<b>Whole crystal</b>								<b>223.26</b>	<b>234.77</b>	<b>458.02</b>

### 3.1.1. $\alpha$ -form

The calculated particle surface energies indicate that the total surface energy of the  $\alpha$ -form morphology was calculated to be 221.91 mJ

m<sup>-2</sup>, lower than that calculated for the total particle surface energy of  $\beta$ -form, which was 458.02 mJ m<sup>-2</sup> both highlighted in red in Table 1. The  $\{111\}$  surface of the  $\alpha$  polymorph was found to contribute 85.6 %

of the total particle surface energy and the remaining 14.4 % by the {0 0 2} surface. The total coulombic contribution to the overall  $\alpha$ -form particle surface energy was calculated to be  $95.00 \text{ mJ m}^{-2}$ , 42.8 % of the total particle surface energy and the dispersive component was found to have a higher contribution,  $126.91 \text{ mJ m}^{-2}$ , 57.2 % of the total particle surface energy.

The calculated surface energy was further supported by a qualitative analysis of the surface chemistry for the  $\alpha$ -form LGA. Fig. 3 a) and b) presents the surface chemistry of the {1 1 1} and {0 0 2} forms of the  $\alpha$  polymorph respectively. This analysis highlights that due to the small, highly charged nature of the glutamic acid molecule there are only subtle differences in the observed surface chemistry at the different surfaces. Almost all conformational rotations of the LGA molecule yield a surface with either a combination of ammonium, carboxylate or acid functionalities present at the surface. In the  $\alpha$  polymorph, the {1 1 1} surface has alternating combinations of ammonium and acid functionalities present; together with carboxylate functionalities which are twisted away from the surface normal. The {0 0 2} surface has carboxylate and acid groups available at the surface however the ammonium groups are not exposed on the surface topography (Fig. 3 b)), hence inaccessible. This seems to correlate with the calculated surface energy in Table 1, where for the  $\alpha$  polymorph, there is little variation between the relative contribution of the coulombic and dispersive components at the two surfaces, and also that the surface energy of the two forms are reasonably isotropic;  $\gamma_{Total} = 219.12$  and  $240.10 \text{ mJ m}^{-2}$  for the {1 1 1} and {0 0 2} respectively.

### 3.1.2. $\beta$ -form

A consequence of the thin needle-like morphology of the  $\beta$  polymorph is that the {0 0 2} surface contribution of 91.8 % dominates the total particle surface energy, whereas the {1 1 1} and {0 1 1} surfaces contribute only 1.0 % and 7.2 % respectively. This resulted in the high coulombic component of the {0 0 2} surface energy dominating the

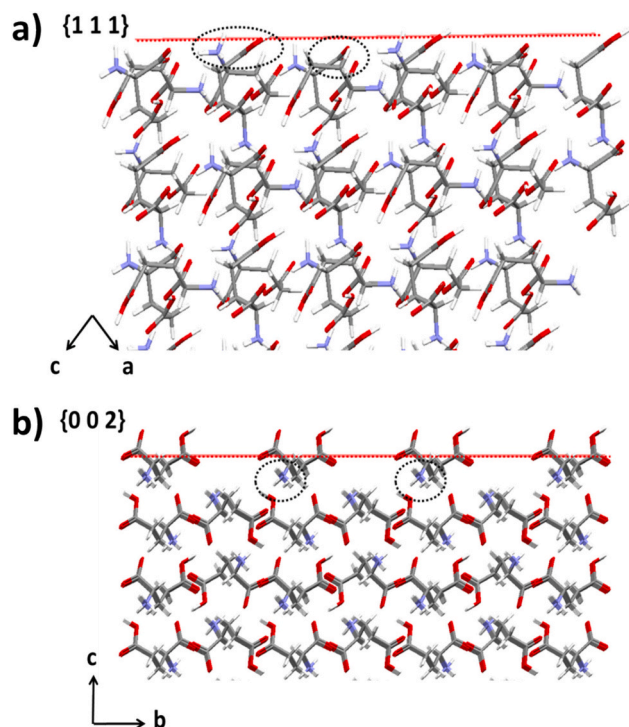


**Fig. 3.** The surface chemistry of the  $\alpha$ -form LGA: a) the {1 1 1} surface and b) the {0 0 2} surface, highlighting the alternating ammonium and carboxylate groups exposed on the {1 1 1} surface and in contrast the ammonium group unexposed on the {0 0 2} surface (hence inaccessible) with the carboxylate and carboxylic acid groups exposed on this surface.

overall particle surface energy and hence the coulombic contribution in the  $\beta$  polymorph is  $234.77 \text{ mJ m}^{-2}$ , 51.1 % of the total particle surface energy and the dispersive component contributed  $223.36 \text{ mJ m}^{-2}$ , 48.9 % of the overall total particle surface energy, as highlighted in Table 1. The overall conclusions drawn from this analysis are firstly that the calculated particle surface energy of  $\alpha$ -form LGA was lower than that of the  $\beta$ -form, and secondly that the overall particle surface energy of the  $\alpha$ -form was found to be dominated by the dispersive component whereas the coulombic component in the  $\beta$ -form was found to make slightly larger contribution to the overall particle surface energy.

Fig. 4 a), b) and c) highlights the surface chemistry of the {0 0 2}, {1 1 1} and {0 1 1} faces of the  $\beta$  polymorph respectively. The {0 0 2} surface was found to have a high plane rugosity, providing low energy binding sites for solvent water [50], and contain acid groups protruding from the surface, additionally the carboxylate and ammonium groups are located within the surface valleys and these are highlighted in Fig. 4a). This correlates well with the calculated  $\gamma_{Total}$  of the {0 0 2} plane of  $490.10 \text{ mJ m}^{-2}$ , relative to the other  $\beta$ -form surfaces. In comparison the {1 1 1} and {0 1 1} surfaces have no acid or charged groups which are directly perpendicular to the surface and this correlates well with the lower calculated  $\gamma_{Total}$  of  $218.69$  and  $272.31 \text{ mJ m}^{-2}$  respectively.

### 3.2. Experimentally determined surface energies

Table 2 and Fig. 5(a) summarise the surface energy data obtained

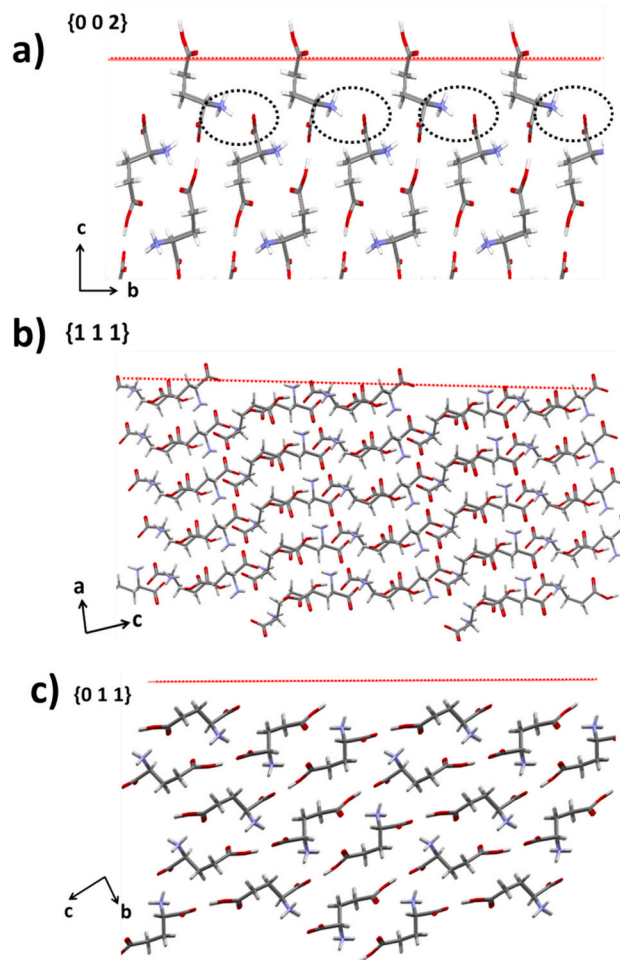


**Fig. 4.** The surface chemistry of the  $\beta$ -form LGA: a) the {0 0 2} surface where the carboxylate and ammonium groups are highlighted within the surface valleys, b) the {1 1 1} surface and c) the {0 1 1} surface.

**Table 2**

The measured total surface energy of the  $\alpha$  and  $\beta$  polymorphs of L-glutamic acid and the deconvolution into dispersive and polar components through contact angle measurements using Washburn Capillary Rise method and inverse gas chromatography measurements.

Surface Energy	Washburn Capillary Rise		Inverse Gas Chromatography	
	$\alpha$ -LGA	$\beta$ -LGA	$\alpha$ -LGA	$\beta$ -LGA
Total Surface Energy ( $\text{mJ m}^{-2}$ )	29.20	36.20	43.11	48.24
Dispersive Component ( $\text{mJ m}^{-2}$ )	15.10	16.90	41.62	43.25
Polar Component ( $\text{mJ m}^{-2}$ )	14.10	19.40	1.48	4.99

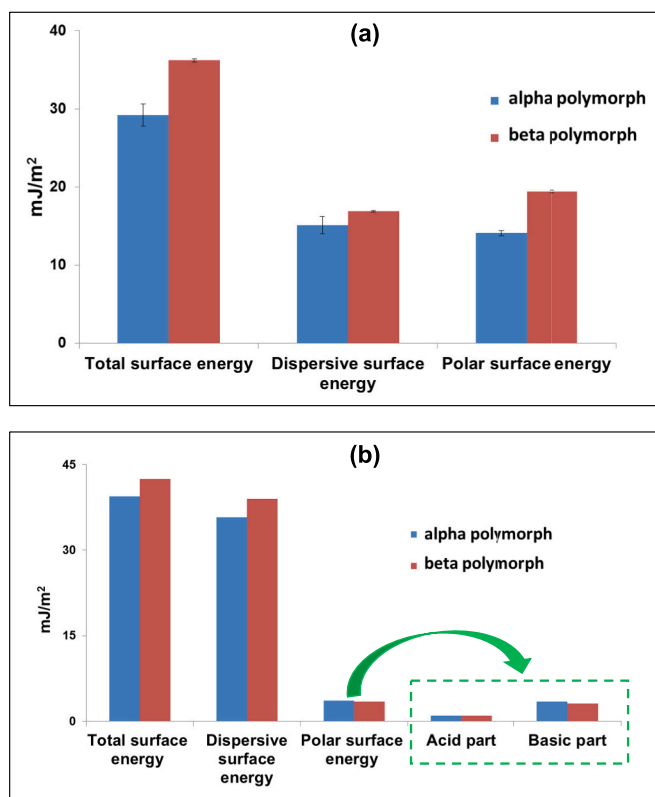


**Fig. 5.** Experimentally determined surface energy for the alpha (blue) and beta (red) polymorphic forms of LGA: a) by Washburn capillary rise, with the total surface energy being de-convoluted into dispersive and polar components; b) by inverse gas chromatography, with the total surface energy being further distributed into dispersive, polar, acid and base components. (For interpretation of the references to colour in this figure legend, the reader is referred to the web version of this article.)

from the capillary rise experiments, where the total surface energy was calculated to be  $29.20 \text{ mJ m}^{-2}$  for the  $\alpha$  polymorph and  $36.20 \text{ mJ m}^{-2}$  for the  $\beta$  polymorph. The interaction of the water solvent probe with the powdered samples of  $\alpha$ - and  $\beta$ -forms revealed that the polar surface energy of the  $\beta$ -form to be  $19.40 \text{ mJ m}^{-2}$ , higher than that of the  $\alpha$ -form which was calculated to be  $14.10 \text{ mJ m}^{-2}$ . The interaction of the diiodomethane solvent with the powdered samples allowed calculation of the dispersive surface energy component which was found to be  $15.10 \text{ mJ m}^{-2}$  for the  $\alpha$  polymorph and  $16.90 \text{ mJ m}^{-2}$  for the  $\beta$  polymorph.

The trends in the surface energy data calculated using the capillary rise technique correlate well with the modelled surface energy using the particle surface area corrected method. The  $\beta$  polymorph was predicted to have the higher total surface energy and the experimental data agrees well in this regard, with good separation in total energy values calculated between the two powders. Additionally, the modelling data predicted that the surface energy of the  $\alpha$  polymorph to have a higher

contribution of the dispersive component relative to the polar component and the experimental data set also shows this trend. Moreover, the  $\beta$  polymorph was predicted to have a higher contribution from the polar component relative to the dispersive component to its total surface energy, and this was also found in the experimental data set.

The surface energy analysis of the bulk powders of both forms as measured using the IGC method is shown in Table 2 and Fig. 5(b). The data indicates that the total surface energy of the  $\beta$ -form to be higher than that of the  $\alpha$  form;  $48.24 \text{ mJ m}^{-2}$  for  $\beta$ -form and  $43.11 \text{ mJ m}^{-2}$  for  $\alpha$ -form. This finding is in agreement with the calculated values of surface energy of LGA where the  $\beta$ -form was found to have a higher total surface energy.

### 3.3. Comparison between prediction and experimental data

It is noteworthy that the values of the experimentally determined total surface energies are lower than that predicted based upon the attachment energy data detailed in Table 1. In general, these differences reflect the same trend as those found in studies of D-mannitol [46,47]. The discrepancy is likely due to a number of factors, most notably the fundamental differences between the basis for the experimental determination and theoretical calculation. One key difference is that the theoretical model predicts the surface energy of the crystal habit planes terminated within a vacuum environment, i.e. without solvent binding. This is in contrast with the experimental data which has been carried out under positive gaseous pressure using the IGC method or within a solution environment using the Washburn capillary rise method. A further issue is that the experimental surface energy measurements may not achieve sufficient surface coverage in order to visit and take into account all the lowest surface-energy sites [48]. The crystal habit faces used for surface energy calculations also assume the modelled surface to be a perfectly cleavage of the bulk crystallographic structure i.e. atomically smooth and with no step/kink sites, no surface contamination by the inclusion of impurities, and a perfect surface structure i.e. without any defects such as dislocations.

More specifically, with respect to the current study, the modelling on LGA reflects theoretical calculations for an organic material with a zwitterionic and hence very polar bulk and surface chemistry for both polymorphs. Previous work by Turner et al. [50], summarised in Table 3, reveals the extrinsic surface terminated synthons for the several crystal habit surfaces involve zwitterionic interactions between the polar  $\text{NH}^+$  and  $\text{COOH}^-$  groups. Thermodynamically it would be quite unlikely that such ‘dangling synthons’ would be structurally stable without some degrees of adsorption such as solvation and/or structural re-organisation to minimise surface energy. In the former case solvent binding studies on the LGA crystal habit surfaces have revealed very strong interactions with solvation water molecules, particularly with those facets involving surface-terminated zwitterionic interactions. Clearly, further work is needed to gain a better understanding of the surface termination effects for such polar systems. Recent studies on the markedly less polar alpha lactose monohydrate system [49] where dispersive interactions are much stronger reveal a much closer correspondence between predicted and measured surface energies.

For future studies, manually introducing heteromolecular contaminations and/or imperfections to the habit faces when predicting the surface energies may prove to be more realistic in order to mimic the real conditions under IGC or WCR measurement conditions, hence leading to more comparable surface energies between those predicted and measured.

## 4. Conclusions

A methodology together with an underpinning integrated experimental and computational workflow has been presented for the prediction and validation of crystal surface energy on a face-specific basis and, through this, on a particulate basis. The approach fuses particle

**Table 3**  
The extrinsic bulk synthons for the several habit surfaces to involve strong surface-terminated zwitterionic interactions between the  $\text{NH}_3^+$  and  $\text{COOH}^-$  groups.

Bond	Intermolecular Energy / kcal mol <sup>-1</sup>	H-Bond Distance / Å	% Contribution to $E_{\text{air}}$	Intermolecular H-Bond Interaction	Charge Type	Contribution for Synthon Multiplicity to $E_{\text{air}}$ on Habit Surfaces		
						Basel face {002}	Pyramidal face {111}	Capping face {111}
<i>α polymorph</i>								
Aα	-6.70	2.85	32.03	$\text{COO}^- \cdots \text{NH}_3^+$	Zwitterionic	0	2	2
Bα	-4.32	2.86	20.66	$\text{COO}^- \cdots \text{NH}_3^+$	Zwitterionic	2	2	2
Cα	-3.75	2.90	17.93	$\text{NH}_3^+ \cdots \text{O}=\text{C}$	Regular	2	2	2
Dα	-3.04	2.93	14.54	$\text{OH} \cdots \text{COO}^-$	Regular	2	2	2
			<b>Total 85.15</b>					
<i>β polymorph</i>								
Aβ	-5.88	2.73	27.33	$\text{COO}^- \cdots \text{NH}_3^+$	Zwitterionic	0	2	2
Bβ	-5.36	2.68	24.91	$\text{COO}^- \cdots \text{NH}_3^+$	Zwitterionic	0	2	2
Cβ	-4.14	2.87	19.24	$\text{OH} \cdots \text{COO}^-$	Regular	4	2	2
Dβ	-2.25	2.81	10.46	$\text{COO}^- \cdots \text{NH}_3^+$	Zwitterionic	0	0	4
			<b>Total 81.94</b>					

surface energies are calculated through the summation of the contributions from individual surfaces of faceted crystal through their respective weighting by their fractional surface areas. The approach quantifies the anisotropy of crystal surface properties including their dispersive and coulombic contributions. The workflow provides useful insight as to how the surface chemistry of individual habit faces impact upon surface behaviour during ingredient preparation, formulation processing and, ultimately, product performance. Through this, it provides a valuable resource for the powder-based digital design of formulated products.

Calculating the surface energies of faceted organic crystals on a face-specific and whole particle basis for the two polymorphic forms of LGA has been shown to provide a rank order prediction of surface energy together with its dispersive to coulombic contributions relative to the established experimental methods of IGC and WCR. The calculated values of surface energies match the same overall trend as those found from experimental studies albeit with higher values with respect to the experimental values, which are consistent with the previous literature findings [46]. The discrepancy between the theoretical calculations and experimental measurements most likely reflects fundamental differences between the environments underpinning the experimental and prediction conditions, such as a vacuum for prediction, under positive pressure for IGC and solvated for WCR. Through further improvements in the modelling methodologies, these could be addressed in future work.

The approach and its integrated workflow are highly aligned with the industry drivers around obtaining better control of the API:DP interface needed for industrial digital transformation towards simulation-based digital design. This could have utility for the early stages of the drug product development cycle mindful that the approach only requires crystal structural information which can be readily available from small quantities of material or potentially predicted. This would be in contrast to experimentally-based empirical modelling that can require grams to kg amounts of material. The modelling-based workflow also has benefits, in that it provides improved granularity through the provision of the face-specific particulate properties important in digital product design. The method is also quite rapid compared to e.g., IGC methods where covering a range of dispersive and polar probe molecules can take a number of days. A further advantage reflects the ability of the modelling approach to examine a wide range of probe molecules, particularly e.g. polar probes that might not be suitable e.g. for volatilisation for IGC analysis or those which can be corrosive. Overall, the surface energies calculated when compared to other polymorphic forms or morphologies of an API could be used to provide insights into the fundamental aspects of formulation design as well as down-stream processability and performance in the drug product.

#### CRedit authorship contribution statement

**Thomas D. Turner:** Writing – review & editing, Writing – original draft, Visualization, Methodology, Investigation, Formal analysis, Data curation, Conceptualization. **Cai Y. Ma:** Writing – review & editing, Writing – original draft, Visualization, Conceptualization. **Yuosef Al Ayoub:** Methodology, Formal analysis, Data curation. **Radoslav Y. Penchev:** Writing – review & editing, Methodology, Data curation, Conceptualization. **Neil Dawson:** Writing – review & editing, Supervision, Conceptualization. **Martyn Ticehurst:** Writing – review & editing, Supervision, Conceptualization. **Robert Docherty:** Writing – review & editing, Supervision, Funding acquisition, Conceptualization. **Kevin J. Roberts:** Writing – review & editing, Writing – original draft, Supervision, Methodology, Funding acquisition, Formal analysis, Conceptualization.

#### Declaration of competing interest

The authors declare that they have no known competing financial

interests or personal relationships that could have appeared to influence the work reported in this paper.

## Data availability

Data will be made available on request.

## Acknowledgements

This work was funded by the Advanced Manufacturing Supply Chain Initiative 'Advanced Digital Design of Pharmaceutical Therapeutics' (ADDoPT) project (Grant No. 14060) in collaboration with AstraZeneca, Bristol-Myers Squibb, BRITEST, Cambridge Crystallographic Data Centre, GSK, Perceptive Engineering, Pfizer, Process Systems Enterprise and the STFC Hartree Centre together with the Universities of Cambridge and Strathclyde. This work also builds upon research on morphological modelling supported by EPSRC grant 'HABIT – Crystal morphology from crystallographic and growth environment factors' through EPSRC grant EP/I028293/1 and the Synthonic Engineering programme supported by Pfizer, Boeringer-Ingellheim, Novartis and Syngenta. We also gratefully acknowledge EPSRC for the support of Crystallisation Research at Leeds and Manchester through the Critical Mass grant 'Molecules, Clusters and Crystals' (Grant references EP/I014446/1 and EP/I013563/1). We are grateful to the EPSRC for the financial support of the Future Continuous Manufacturing and Advanced Crystallisation (CMAC) Research Hub (Grant EP/P006965/1).

## References

- N. Anuar, S.N. Yusop, K.J. Roberts, Crystallisation of organic materials from the solution phase: a molecular, synthonic and crystallographic perspective, *Crystallogr. Rev.* 28 (2022) 97–215.
- R. Docherty, G. O'Connor, R.Y. Penchev, J. Pickering, V. Ramachandran, From molecules to crystals to functional form: Science of scale. Chap. 29, in: K.J. Roberts, R. Docherty, R. Temura (Eds.), *Engineering Crystallography: From Molecule to Crystal to Functional Form*, Springer VCH, Dordrecht, The Netherlands, 2017, pp. 463–478.
- M.D. Ticehurst, I. Marziano, Integration of active pharmaceutical ingredient solid form selection and particle engineering into drug product design, *J. Pharm. Pharmacol.* 67 (2015) 782–802.
- ADDoPT, ADDoPT Case Studies, 2019.
- R. Docherty, Digital Design, Medicines Manufacturing Industry Partnership (MMIP) Conference, Sandwich, UK, 2019.
- R. Docherty, K.J. Roberts, White paper on gaps and obstacles in materials modelling, in: EMMC-CSA – GA N°723867. Deliverable Report D1.4 - White paper on gaps and obstacles in materials modelling Pharma Materials, 2019.
- K.J. Roberts, R.B. Hammond, V. Ramachandran, R. Docherty, Synthonic engineering: From molecular and crystallographic structure to the rational design of pharmaceutical solid dosage forms, in: Y.A. Abramov (Ed.), *Computational Approaches in Pharmaceutical Solid State Chemistry*, John Wiley & Sons, Ltd, 2015, pp. 175–210.
- V. Ramachandran, D. Murnane, R.B. Hammond, J. Pickering, K.J. Roberts, M. Soufian, B. Forbes, S. Jaffari, G.P. Martin, E. Collins, Formulation pre-screening of inhalation powders using computational atom-atom systematic search method, *Mol. Pharm.* 12 (2015) 18–33.
- C.Y. Ma, T.T.H. Nguyen, P. Gajjar, I.D. Styliari, R.B. Hammond, P.J. Withers, D. Murnane, K.J. Roberts, Predicting the strength of cohesive and adhesive Interparticle interactions for dry powder inhalation blends of terbutaline sulfate with  $\alpha$ -lactose monohydrate, *Mol. Pharm.* 20 (2023) 5019–5031.
- M. Kitamura, Polymorphism in the crystallization of L-glutamic acid, *J. Cryst. Growth* 96 (1989) 541–546.
- Y. Huo, D. Guan, Size measurement and prediction for L-glutamic acid crystal growth during stirred crystallization based on imaging analysis, *Math. Biosci. Eng.* 18 (2021) 1864–1878.
- Z. Gao, Y. Wu, Y. Ying Bao, J. Gong, J. Wang, S. Rohani, Image analysis for in-line measurement of multidimensional size, shape, and polymorphic transformation of L-glutamic acid using deep learning-based image segmentation and classification, *Cryst. Growth Des.* 18 (2018) 4275–4281.
- Y. Tahri, E. Gagnière, E. Chabanon, T. Bounahmidi, D. Mangin, Investigation of the L-glutamic acid polymorphism: comparison between stirred and stagnant conditions, *J. Cryst. Growth* 435 (2016) 98–104.
- Y. Huo, T. Liu, H. Liu, C.Y. Ma, X.Z. Wang, In-situ crystal morphology identification using imaging analysis with application to the L-glutamic acid crystallization, *Chem. Eng. Sci.* 148 (2016) 126–139.
- D.R. Ochsenein, S. Schorsch, F. Salvatori, T. Vetter, M. Morari, M. Mazzotti, Modeling the facet growth rate dispersion of  $\beta$  L-glutamic acid—combining single crystal experiments with nD particle size distribution data, *Chem. Eng. Sci.* 133 (2015) 30–43.
- D.R. Ochsenein, S. Schorsch, T. Vetter, M. Mazzotti, M. Morari, Growth rate estimation of  $\beta$  L-glutamic acid from online measurements of multidimensional particle size distributions and concentration, *Ind. Eng. Chem. Res.* 53 (2014) 9136–9148.
- C.Y. Ma, X.Z. Wang, Model identification of crystal facet growth kinetics in morphological population balance modeling of L-glutamic acid crystallization and experimental validation, *Chem. Eng. Sci.* 70 (2012) 22–30.
- M.W. Hermanto, N.C. Kee, R.B.H. Tan, M.-S. Chiu, R.D. Braatz, Robust Bayesian estimation of kinetics for the polymorphic transformation of L-glutamic acid crystals, *AIChE J.* 54 (2008) 3248–3259.
- X.Z. Wang, J. Calderon De Anda, K.J. Roberts, Real-time measurement of the growth rates of individual crystal facets using imaging and image analysis: a feasibility study on needle-shaped crystals of L-glutamic acid, *Chem. Eng. Res. Des.* 85 (2007) 921–927.
- J. Scholl, C. Lindenberg, L. Vicum, J. Brozio, M. Mazzotti, Precipitation of a L-glutamic acid: determination of growth kinetics, *Faraday Discuss.* 136 (2007) 247–264.
- C.Y. Ma, X.Z. Wang, K.J. Roberts, Multi-dimensional population balance modeling of the growth of rod-like L-glutamic acid crystals using growth rates estimated from in-process imaging, *Adv. Powder Technol.* 18 (2007) 707–723.
- R.F. Li, G.B. Thomson, G. White, X.Z. Wang, J. Calderon De Anda, K.J. Roberts, Real-time product morphology monitoring in crystallization using imaging technique, *AIChE J.* 52 (2006) 2297–2305.
- R.B. Hammond, K. Pencheva, K.J. Roberts, Simulation of energetic stability of faceted L-glutamic acid nanocrystalline clusters in relation to their polymorphic phase stability as a function of crystal size, *J. Phys. Chem. B* 109 (2005) 19550–19552.
- J. Calderon De Anda, X.Z. Wang, K.J. Roberts, K.H. Jennings, M.J. Wilkinson, D. Watson, D. Roberts, Real-time product morphology monitoring in crystallization using imaging technique, *AIChE J.* 51 (2005) 1406–1414.
- T. Ono, H.J.M. Kramer, J.H. ter Horst, P.J. Jansens, Process modeling of the polymorphic transformation of L-glutamic acid, *Cryst. Growth Des.* 4 (2004) 1161–1167.
- K. Liang, G. White, D. Wilkinson, L.J. Ford, K.J. Roberts, W.M.L. Wood, Examination of the process scale dependence of L-glutamic acid batch crystallized from supersaturated aqueous solutions in relation to reactor hydrodynamics, *Ind. Eng. Chem. Res.* 43 (2004) 1227–1234.
- K. Liang, G. White, D. Wilkinson, L.J. Ford, K.J. Roberts, W.M.L. Wood, An examination into the effect of stirrer material and agitation rate on the nucleation of L-glutamic acid batch crystallized from supersaturated aqueous solutions, *Cryst. Growth Des.* 4 (2004) 1039–1044.
- M. Kitamura, T. Ishizu, Growth kinetics and morphological change of polymorphs of L-glutamic acid, *J. Cryst. Growth* 209 (2000) 138–145.
- S. Khan, C.Y. Ma, T. Mahmud, P.Y. Penchev, K.J. Roberts, J. Morris, L. Özkan, G. White, B. Grieve, A. Hall, P. Buser, N. Gibson, P. Keller, P. Shuttleworth, C. J. Price, In-process monitoring and control of supersaturation in seeded batch cooling crystallisation of L-glutamic acid: from laboratory to industrial pilot plant, *Org. Process Res. Dev.* 15 (2011) 540–555.
- M. Kitamura, T. Ishizu, Kinetic effect of L-phenylalanine on growth process of L-glutamic acid polymorph, *J. Cryst. Growth* 192 (1998) 225–235.
- C. Jiang, C.Y. Ma, T.A. Hazlehurst, T.P. Ilett, A.S.M. Jackson, D.C. Hogg, K. J. Roberts, Automated growth rate measurements of the facet surfaces of single crystals of the  $\beta$ -form L-glutamic acid using machine learning image processing, *Cryst. Growth Des.* 24 (2024) 3277–3288.
- C.Y. Ma, C. Jiang, T.P. Ilett, T.A. Hazlehurst, A.S.M. Jackson, D.C. Hogg, K. J. Roberts, Deconstructing 3D faceted crystal growth rates from optical microscopy data captured in-situ within supersaturated aqueous solution, *J. Appl. Crystallogr.* (2024), <https://doi.org/10.1107/S1600576724008173>.
- K. Wu, C.Y. Ma, J.J. Liu, Y. Zhang, X.Z. Wang, Measurement of crystal face specific growth kinetics, *Cryst. Growth Des.* 16 (2016) 4855–4868.
- J. Calderon De Anda, X.Z. Wang, K.J. Roberts, Classifying organic crystals via in-process image analysis and the use of monitoring charts to follow polymorphic and morphological changes, *J. Process Control* 15 (2005) 785–797.
- J. Calderon De Anda, X.Z. Wang, K.J. Roberts, Multi-scale segmentation image analysis for the in-process monitoring of particle shape with batch crystallisers, *Chem. Eng. Sci.* 60 (2005) 1053–1065.
- R.F. Li, R. Penchev, V. Ramachandran, K.J. Roberts, X.Z. Wang, Particle shape characterisation via image analysis: from laboratory studies to in-process measurements using an in situ particle viewer system, *Org. Process Res. Dev.* 12 (2008) 837–849.
- G. Clydesdale, R. Docherty, K. Roberts, HABIT95 - a program for predicting the morphology of molecular crystals as a function of the growth environment, *J. Cryst. Growth* 166 (1996) 78–83.
- G. Clydesdale, R. Docherty, K.J. Roberts, HABIT - a program for predicting the morphology of molecular crystals, *Comput. Phys. Commun.* 64 (1991) 311–328.
- I. Rosbottom, T.D. Turner, C.Y. Ma, R.B. Hammond, K.J. Roberts, C.W. Yong, I. T. Todorov, The structural pathway from its solvated molecular state to the solution crystallisation of the  $\alpha$ - and  $\beta$ -polymorphic forms of Para amino benzoic acid, *Faraday Discuss.* 235 (2022) 467–489.
- I. Rosbottom, C.W. Yong, D.L. Geatches, R.B. Hammond, I.T. Todorov, K.J. Roberts, The integrated DL, POLY/DL, FIELD/DL, ANALYSER software platform for molecular dynamics simulations for exploration of the synthonic interactions in saturated benzoic acid/hexane solutions, *Mol. Simul.* 47 (2021) 257–272.

- [41] D. Toroz, I. Rosbottom, T.D. Turner, D.M.C. Corzo, R.B. Hammond, X. Lai, K. J. Roberts, Towards an understanding of the nucleation of alpha-Para amino benzoic acid from ethanolic solutions: a multi-scale approach, *Faraday Discuss.* 179 (2015) 79–114.
- [42] C. Wang, C.Y. Ma, R. Hong, T.D. Turner, I. Rosbottom, A. Sheikh, Q. Yin, K. J. Roberts, Influence of solvent selection on the crystallisability and polymorphic selectivity associated with the formation of the “disappeared” form I polymorph of ritonavir, *Mol. Pharm.* 21 (2024) 3525–3539.
- [43] I. Rosbottom, T.D. Turner, C.Y. Ma, R.B. Hammond, K.J. Roberts, C.W. Yong, I. T. Todorov, The structural pathway from its solvated molecular state to the solution crystallisation of the  $\alpha$ - and  $\beta$ -polymorphic forms of Para amino benzoic acid, *Faraday Discuss.* 235 (2022) 467–489.
- [44] F. Giberti, M. Salvalaglio, M. Parrinello, Metadynamics studies of crystal nucleation, *JUCrJ* 2 (2015) 256–266.
- [45] M. Salvalaglio, G. Perego, F. Giberti, M. Mazzotti, M. Parrinello, Molecular-dynamics simulations of urea nucleation from aqueous solution, *Proc. Natl. Acad. Sci.* 112 (2015) E6–E14.
- [46] N. Di Pasquale, R.L. Davidchack, Cleaving method for molecular crystals and its application to calculation of the surface free energy of crystalline  $\beta$ -D-mannitol at room temperature, *Chem. Eur. J.* 126 (2022) 2134–2141.
- [47] R. Ho, S.J. Hinder, J.F. Watts, S.E. Dilworth, D.R. Williams, J.Y.Y. Heng, Determination of surface heterogeneity of D-mannitol by sessile drop contact angle and finite concentration inverse gas chromatography, *Int. J. Pharm.* 387 (2010) 79–86.
- [48] T.T.H. Nguyen, R.B. Hammond, I.D. Styliari, D. Murnane, K.J. Roberts, A digital workflow from crystallographic structure to single crystal particle attributes for predicting the formulation properties of terbutaline sulfate, *CrystEngComm* 22 (2020) 3347–3360.
- [49] T.T.H. Nguyen, C.Y. Ma, I.D. Styliari, P. Gajjar, R.B. Hammond, P.J. Withers, D. Murnane, K.J. Roberts, Structure, morphology and surface properties of crystalline  $\alpha$  lactose monohydrate in relation to powder cohesion, agglomeration and compaction, *J. Pharm. Sci.* (2024) (under review).
- [50] T.D. Turner, N. Dawson, M. Edwards, J.H. Pickering, R.B. Hammond, R. Docherty, K.J. Roberts, A digital mechanistic workflow for predicting solvent-mediated crystal morphology: the  $\alpha$  and  $\beta$  forms of L-glutamic acid, *Cryst. Growth Des.* 22 (2022) 3042–3059.
- [51] R. Ho, J.Y.Y. Heng, A review of inverse gas chromatography and its development as a tool to characterize anisotropic surface properties of pharmaceutical solids, *Kona Powd. Part. J.* 30 (2013) 164–180.
- [52] P. Klitou, I. Rosbottom, V. Karde, J.Y.Y. Heng, E. Simone, Relating crystal structure to surface properties: a study on quercetin solid forms, *Cryst. Growth Des.* 22 (2022) 6103–6113.
- [53] R. Ho, J.Y.Y. Heng, S.E. Dilworth, D.R. Williams, Wetting behavior of ibuprofen Racemate surfaces, *J. Adhes.* 84 (2008) 483–501.
- [54] S. Kirdponpattara, M. Phisalaphong, B.Z. Newby, Applicability of Washburn capillary rise for determining contact angles of powders/porous materials, *J. Colloid Interface Sci.* 397 (2013) 169–176.
- [55] J.Y.Y. Heng, A. Bismarck, D.R. Williams, Anisotropic surface chemistry of crystalline pharmaceutical solids, *AAPS PharmSciTech* 7 (2006) E12–E20.
- [56] D. Zhang, J.H. Flory, S. Panmai, U. Batra, M.J. Kaufman, Wettability of pharmaceutical solids: its measurement and influence on wet granulation, *Wettability of pharmaceutical solids: its measurement and influence on wet granulation*, *Colloids Surf. A Physicochem. Eng. Asp.* 206 (2002) 547–554.
- [57] D. Cline, R. Dalby, Predicting the quality of powders for inhalation from surface energy and area, *Pharm. Res.* 19 (2002) 1274–1277.
- [58] S.C. Das, I.G. Tucker, P.J. Stewart, Surface energy determined by inverse gas chromatography as a tool to investigate particulate interactions in dry powder inhalers, *Curr. Pharm. Des.* 21 (2015) 3932–3944.
- [59] D. Traini, P. Rogueda, P. Young, R. Price, Surface energy and interparticle forces correlations in model pMDI formulations, *Pharm. Res.* 22 (2005) 816–825.
- [60] M.D. Jones, P. Young, D. Traini, The use of inverse gas chromatography for the study of lactose and pharmaceutical materials used in dry powder inhaler, *Adv. Drug Deliv. Rev.* 64 (2012) 285–293.
- [61] H.H. Tong, B.Y. Shekunov, P. York, A.H. Chow, Predicting the aerosol performance of dry powder inhalation formulations by interparticulate interaction analysis using inverse gas chromatography, *J. Pharm. Sci.* 95 (2006) 228–233.
- [62] E. Hadjittofis, G.G. Zhang, J.Y.Y. Heng, Influence of sample preparation on IGC measurements: the cases of silanised glass wool and packing structure, *RSC Adv.* 7 (2017) 12194–12200.
- [63] V. Swaminathan, J. Cobb, I. Saracovan, Measurement of the surface energy of lubricated pharmaceutical powders by inverse gas chromatography, *Int. J. Pharm.* 312 (2006) 158–165.
- [64] G. Garnier, W.G. Glasser, Measurement of the surface energy of lubricated pharmaceutical powders by inverse gas chromatography, *J. Adhes.* 46 (1994) 165–180.
- [65] S.P. Chamrathy, R. Pinal, M.T. Carvajal, Elucidating raw material variability—importance of surface properties and functionality in pharmaceutical powders, *AAPS PharmSciTech* 10 (2009) 780–788.
- [66] L. Lavielle, J. Schultz, Surface properties of carbon fibers determined by inverse gas chromatography: role of pretreatment, *Langmuir* 7 (1991) 978–981.
- [67] S. Jaffari, B. Forbes, E. Collins, J. Khoo, G.P. Martin, D. Murnane, Evidence for the existence of powder sub-populations in micronized materials: aerodynamic size-fractions of aerosolized powders possess distinct physicochemical properties, *Pharm. Res.* 31 (2014) 3251–3264.
- [68] W. Marcoin, H. Duda, J. Kusz, B. Bzowski, J. Warczewski, *Applied Crystallography Conference*, 1999.
- [69] N. Hirayama, K. Shirahata, Y. Ohashi, Y. Sasada, Structure of  $\alpha$  form of L-glutamic acid,  $\alpha$ - $\beta$  transition, *Bull. Chem. Soc. Jpn.* 53 (1980) 30–35.
- [70] Dassault Systèmes, BIOVIA Materials Studio. <https://www.3ds.com/products-services/biovia/products/molecular-modeling-simulation/biovia-materials-studio/>, 2019, 78946 Vélizy-Villacoublay Cedex, France, 2019.
- [71] S.L. Mayo, B.D. Olafson, W.A. Goddard, DREIDING: a generic force field for molecular simulations, *J. Phys. Chem.* 94 (1990) 8897–8909.
- [72] J. Gasteiger, M. Marsili, A new model for calculating atomic charges in molecules, *Tetrahedron Lett.* 19 (1978) 3181–3184.
- [73] J. Gasteiger, M. Marsili, Iterative partial equalization of orbital electronegativity—a rapid access to atomic charges, *Tetrahedron* 36 (1980) 3219–3228.
- [74] W. Busing, Modeling the phase change in crystalline biphenyl by using a temperature-dependent potential, *Acta Crystallogr. A* 39 (1983) 340–347.
- [75] F.A. Momany, L.M. Carruthers, R.F. McGuire, H.A. Scheraga, Intermolecular potentials from crystal data. III. Determination of empirical potentials and application to the packing configurations and lattice energies in crystals of hydrocarbons, carboxylic acids, amines, and amides, *J. Phys. Chem.* 78 (1974) 1595–1620.
- [76] Mopac Quantum Chemistry Program Exchange Program No. 455. Creative Arts Building 181, Indiana University, Bloomington, IN 47405.
- [77] J. Stewart, MOPAC 6.0, (CQCPE Program# 455). Quantum Chemistry Program Exchange, Creative Arts Building 181, Indiana University, Bloomington, IN, USA, 1983.
- [78] R.B. Hammond, K. Pencheva, K.J. Roberts, Structural variability within, and polymorphic stability of, nano-crystalline molecular clusters of L-glutamic acid and D-mannitol, modelled with respect to their size, shape and ‘crystallisability’, *CrystEngComm* 14 (2012) 1069–1082.
- [79] C.Y. Ma, A. Kwok, D. Getches, Y.-W. Hsiao, K.J. Roberts, Role of molecular, crystal and surface chemistry in directing the crystallisation of Entacapone polymorphs in the presence of templated gold substrates, *Cryst. Growth Des.* 23 (2023) 4522–4537.
- [80] I. Rosbottom, K.J. Roberts, R. Docherty, The solid state, surface and morphological properties of p-aminobenzoic acid in terms of the strength and directionality of its intermolecular synthons, *CrystEngComm* 17 (2015) 5768–5788.
- [81] Y. Liu, C.Y. Ma, J. Gong, K.J. Roberts, Influence of the crystallisation solution environment on the structural pathway from solute solvation to the polymorphic forms of tolfenamic acid, *CrystEngComm* 26 (2024) 4031–4047.
- [82] C. Wang, I. Rosbottom, T.D. Turner, S. Laing, A.G.P. Maloney, A.Y. Sheikh, R. Docherty, Q. Yin, K.J. Roberts, Molecular, solid-state and surface structures of the conformational polymorphic forms of ritonavir in relation to their physicochemical properties, *Pharm. Res.* 38 (2021) 971–990.
- [83] J.S. Chickos, W.E. Acree, Enthalpies of sublimation of organic and organometallic compounds. 1910–2001, *Phys. Chem. Ref. Data* 31 (2002) 537–698.
- [84] K.T. No, K.H. Cho, O.Y. Kwon, M.S. Jhon, H.A. Scheraga, Determination of proton transfer energies and lattice energies of several amino acid zwitterions, *J. Phys. Chem.* 98 (1994) 10742–10749.
- [85] Z. Berkovitch-Yellin, Toward an ab-initio derivation of crystal morphology, *J. Am. Chem. Soc.* 107 (1985) 8239–8253.
- [86] P. Hartman, P. Bennema, The attachment energy as a habit controlling factor: I. Theoretical considerations, *J. Cryst. Growth* 49 (1980) 145–156.
- [87] R.B. Hammond, K. Pencheva, K.J. Roberts, A structural-kinetic approach to model face-specific solution/crystal surface energy associated with the crystallization of acetyl salicylic acid from supersaturated aqueous/ethanol solution, *Cryst. Growth Des.* 6 (2006) 1324–1334.
- [88] R. Docherty, K.J. Roberts, Modelling the morphology of molecular crystals; application to anthracene, biphenyl and  $\beta$ -succinic acid, *J. Cryst. Growth* 88 (1988) 159–168.
- [89] I.J. Bruno, J.C. Cole, P.R. Edgington, M. Kessler, C.F. Macrae, P. McCabe, J. Pearson, R. Taylor, New software for searching the Cambridge structural database and visualizing crystal structures, *Acta Crystallogr. B* 58 (2002) 389–397.
- [90] E. Dowty, Computing and drawing crystal shapes, *Am. Mineral.* 65 (1980) 465–471.
- [91] M.J. Bryant, I. Rosbottom, I.J. Bruno, R. Docherty, C.M. Edge, R.B. Hammond, R. Peeling, J. Pickering, K.J. Roberts, A.G.P. Maloney, “Particle informatics”: advancing our understanding of particle properties through digital design, *Cryst. Growth Des.* 19 (2019) 5258–5266.